ELSEVIER

Journal of Molecular Structure (Theochem) 637 (2003) 55–72

THEO CHEM

www.elsevier.com/locate/theochem

Theoretical study of 2-guanidinobenzimidazole. HF, MP2 and DFT calculations

R.M. Hernández-García[a], N. Barba-Behrens[a], R. Salcedo[c], G. Höjer[b,*]

[a]Departamento de Química Inorgánica, Universidad Nacional Autónoma de México, C.U., 04510 México, D.F., México
[b]Departamento de Física y Química Teórica, Facultad de Química, Universidad Nacional Autónoma de México, C.U., 04510 México, D.F., México
[c]Instituto de Investigaciones en Materiales, Universidad Nacional Autónoma de México, C.U., 04510 México, D.F., México

Received 17 February 2002; revised 29 April 2003; accepted 29 April 2003

Abstract

In this paper, the 2-guanidinobenzimidazole molecular structure is analysed by ab initio (HF and MP2) and density functional theory (DFT) calculations; and the neutral, cationic, and radical forms are studied by ab initio theory. The HF calculations with the 3-21G and 6-31G basis sets provide good geometric features according to available experimental data. The percentage of p-character of the natural atomic hybrids and the charge distribution in the molecule were analysed with the natural bond orbital method (NBO). Calculations of the enthalpy and Gibbs free energies for the protonation reactions of 2-guanidinobenzimidazole were carried out at the HF level. In accordance with the experimental data, UHF/3-21G showed a delocalised free radical.
© 2003 Elsevier B.V. All rights reserved.

Keywords: 2-Guanidinobenzimidazole; Benzimidazole derivative; Ab initio; Density functional theory

1. Introduction

2-Guanidinobenzimidazole (2gb), Fig. 1, has important biological properties, it acts as a stimulator [1] or as an inhibitor [2] of the transport of Na^+ and K^+ in the apical membrane of the skin, it diminishes the gastric acid secretion [3], it acts as a hypoglycemiant [4] and as a hypotensor [5]. Another important property of 2gb is its activity on photosynthesis, it acts as a mild uncoupler of photophosphorylation [6].

2-Guanidinobenzimidazole is a complex molecule, with one benzimidazole and one guanidine group. It is a polyfunctional planar molecule with a delocalised π electronic system. 2gb contains five nitrogen atoms, which may act as basic centres and it has five labile N–H bonds. The basic sites of 2gb have been located using Lewis acids [7] and metallic salts [6]. 2gb acts as a mono- or bi-dentate ligand to form coordination compounds [6–8], stabilizing different geometries and showing photosynthetic activity.

In the 2gb molecule several tautomers (Fig. 2) and isomers (Fig. 3) are possible. The 2gb structure and its dynamical behaviour have been studied in solution by ^{1}H- [9], ^{13}C- [9,10] and ^{15}N- [11] NMR spectroscopy. It was shown that the equivalent conformers **1** and **2**

* Corresponding author. Tel.: +52-55-5622-3804; fax: +52-55-5622-3521.

E-mail address: germund@eros.pquim.unam.mx (G. Höjer).

0166-1280/03/$ - see front matter © 2003 Elsevier B.V. All rights reserved.
doi:10.1016/S0166-1280(03)00370-1

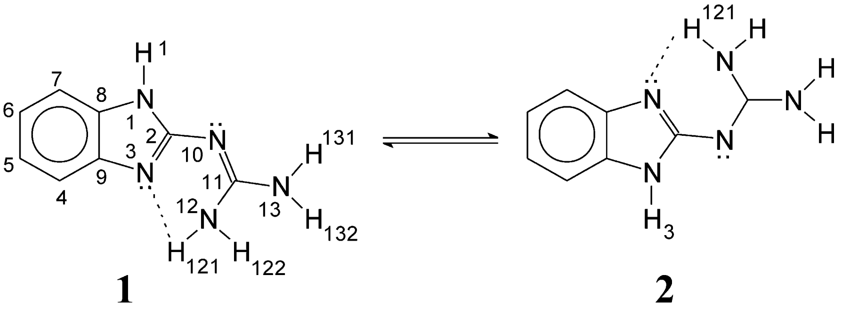

Fig. 1. Conformers **1** and **2** of 2-guanidinobenzimidazole.

(Fig. 1) are the principal contributors. These conformers are in equilibrium and may be stabilized by intramolecular hydrogen bonding [9]. From the X-ray diffraction structure in the solid state [12–14] **1** proved to be the most stable one, displaying intramolecular hydrogen bonding giving rise to a six-member ring.

In Fig. 4 the protonation of 2gb is shown. ^{15}N NMR spectroscopic studies indicated, that the first protonation site occurs at N3 in the cation **3** at any acidity, and the second one at N10 in the cation **4** [7]. Semi-empirical calculations with INDO suggested, that the first protonation site in water is at N10 in the cation **5** [9]. The X-ray diffraction structure of the protonated compound **6**, $[2gb{-}N10H]^{+}AcO^{-}\cdot H_2O$ (Fig. 5), has been published [7], which demonstrated that the protonation occurred at N10.

From EPR spectra, it was found that 2gb stabilizes a delocalised free radical in the molecule **7** (Fig. 6) [15].

The purpose of this study was to analyse the electronic and geometric structures of **1** and its cationic, and radical forms by ab initio (HF and MP2) [16] and density functional theory (DFT) [17] calculations. In a delocalised model structure of 2-guanidinobenzimidazole, the percentage of p-character in the natural atomic hybrids and the charge distribution were analysed by the natural bond orbital (NBO) method [18]. In order to assign the preferred protonation site of 2gb, the imidazole nitrogen N3 or the guanidine nitrogen N10, the cations **3** to **6** were calculated. The enthalpy and Gibbs free energy for the protonation reactions of **1** were calculated at the HF/3-21G and HF/6-31G levels. The free radical was studied at the UHF/3-21G level to determine the localization of the unpaired electron.

2. Computational details

The ab initio calculations were performed using the PC GAMESS version [19a] of the GAMESS (US) package [19b], and the density functional calculations with the GAUSSIAN98 package [20]. Although several basis sets (STO-3G, 3-21G, 6-31G, 6-31G*, 6-31G**, and 6-311G**) were employed to find out the basis set size dependency, mainly the basis sets 3-21G and 6-31G were used throughout most of the calculations. Geometry optimisations were undertaken at various theoretical levels: Hartree–Fock (HF) [16]; second order Møller–Plesset perturbation (MP2) [21]; and Becke's three-parameter hybrid functional using the LYP correlation functional (B3LYP) [22]. The harmonic frequencies were calculated to confirm that the obtained structures were at true minima. In addition, the calculated frequencies were utilised to estimate the zero-point vibrational energies (ZPE) at

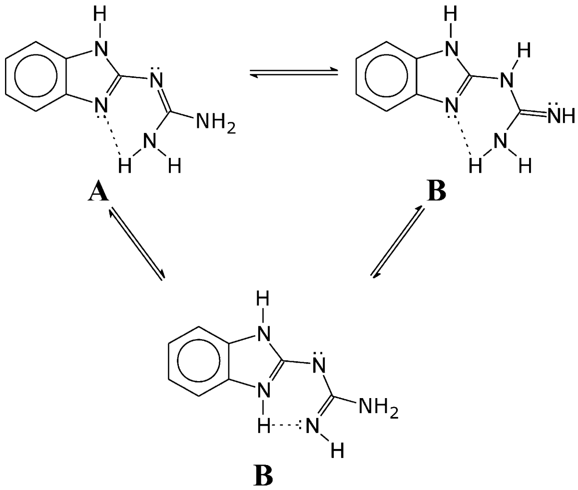

Fig. 2. Tautomers of 2-guanidinobenzimidazole.

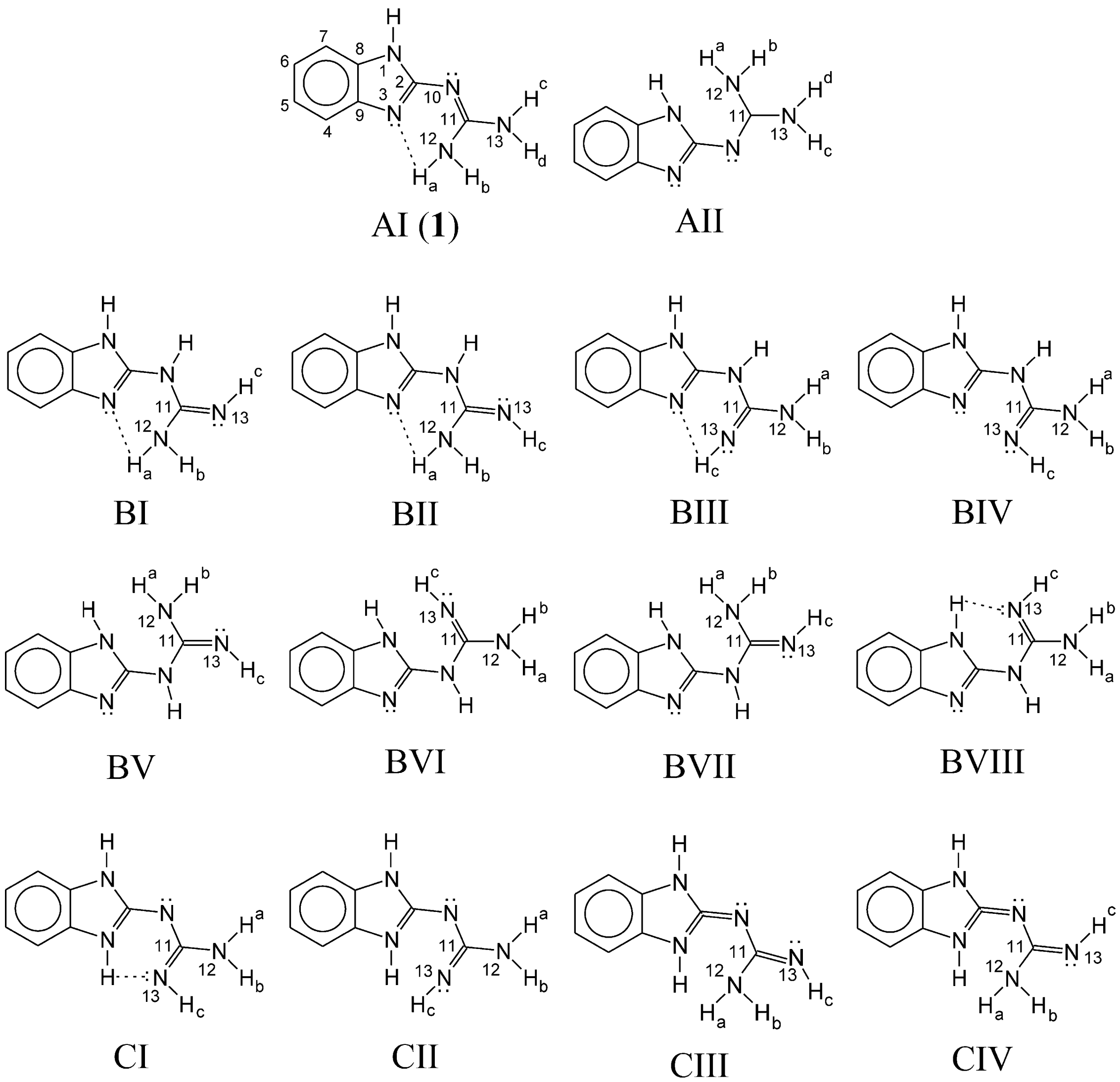

Fig. 3. Isomers of 2-guanidinobenzimidazole.

298 K. In order to investigate the stabilization through vicinal π orbitals, the NBO analysis [23] implemented in both PC GAMESS and GAUSSIAN98 was used. The atomic charges were also calculated with the NBO. The free radical was optimised at the UHF/3-21G level [16]. Initial geometries were obtained by molecular mechanics with the PCMODEL IV package [24]. The structures, molecular orbitals (HOMO and LUMO) and electrostatic potential were visualized with the gOpenMol software and the GAMESS graphics package [25].

3. Results and discussion

3.1. 2-Guanidinobenzimidazole. Conformer **1**

3.1.1. Geometry

The optimised structural parameters and total energies are given in Tables 1 and 2. The experimental X-ray diffraction geometry of the conformer **1** of 2gb has been reported [12–14]. Unfortunately the hydrogen positions could not be determined. We have not found any neutron diffraction results on 2gb in

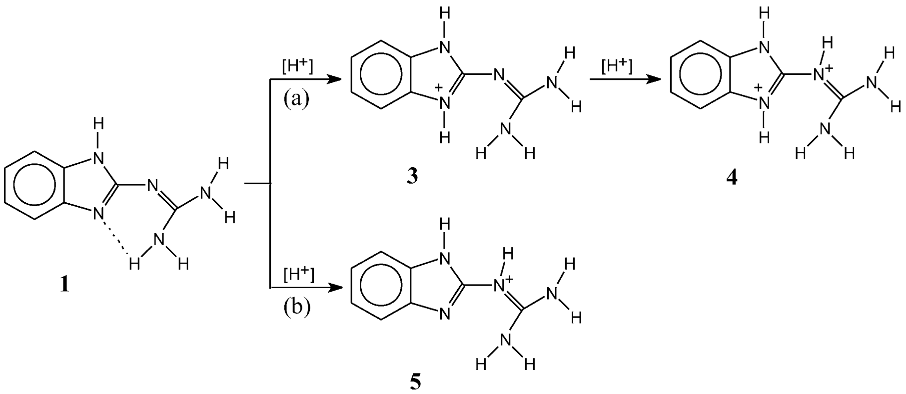

Fig. 4. Protonation of conformer **1**. (a) First protonation on N3 and second protonation on N10 [7,8]. (b) Protonation on N10 [7].

the literature, which could have resolved the hydrogen positions. In Ref. [12] the crystal was a 1:2 complex between 1,4,7,10,13,16-hexaoxacyclooctadecane (18-crown-6) and two 2-guanidinobenzimidazole molecules. The results show essentially planar benzimidazole and guanidine groups (heavy atoms) and an angle between the two planes (the torsion angle 3,2,10,11) of −3.57°. In the more recent paper [14] a pure 2gb crystal was studied. In this case the angle between the planes (the torsion angle 3,2,10,11) was 15.30°. We attribute this large difference in the torsion angle to packing effects in the crystals. Most likely then the isolated 2gb molecule has a planar heavy atom skeleton. Comparing these two experimental structures the average bond length difference was -0.004 Å with standard deviation 0.009 Å and for the bond angles the results were −0.08 and 0.59°. The differences are taken as the values in ref. 12 minus those in ref. 14. The sizes of the variations in the experimental results are important, when the variations in the calculated results are analysed. Finally, the question whether the two amino groups in the guanidine fragment are planar or pyramidal is not experimentally resolved.

The 3-21G and 6-31G basis sets (at the HF and B3LYP levels) predict for **1** a planar geometry for the heavy atom skeleton and planar amino groups in the guanidine fragment. The inclusion of *d* polarization on the heavy atoms (i.e., 6-31G → 6-31G*) favours a conformation with non-planar amino groups in the guanidine fragment. Adding p polarization functions on the hydrogen atoms (6-31G* → 6-31G**) conserves the non-planar amino groups. The non-planarity of these groups is more pronounced with

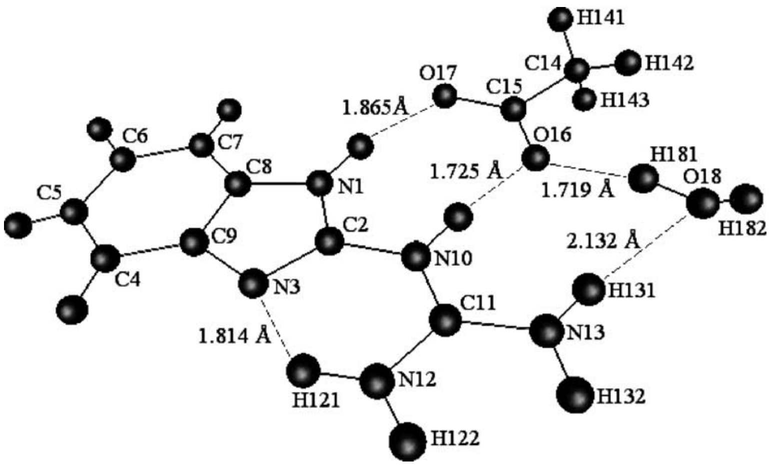

Fig. 5. X-ray diffraction structure of the protonated specie in compound $[2gb–N10H]^{+}AcO^{-}·H_2O$ **6** [7].

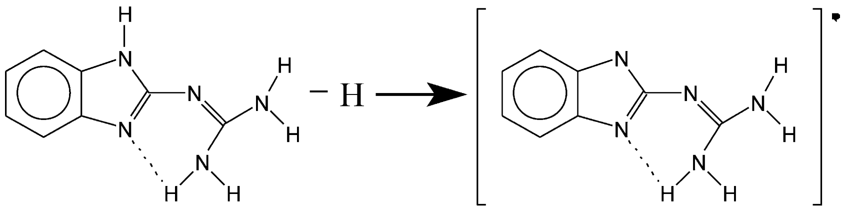

1 **7**

Fig. 6. Radical formation.

the use of large basis sets with polarization, specifically 6-311G* and 6-311G**. The use of polarization functions in DFT, B3LYP/6-31G* leads also to non-planar amino groups. The inclusion of electron correlation in HF at a modest level (MP2/6-31G*, MP2/6-31G**, MP2/6-311G* and MP2/6-311G**, we do not consider it meaningful to make MP2 calculations with smaller basis sets) predicts non-planar amino groups. It is the inclusion of polarization functions and not correlation (MP2 and B3LYP), which determines the non-planarity of the amino groups. A definite answer to this problem would require calculations at a level far beyond the scoop of this work. With the insufficient minimal basis set STO-3G, the largest non-planarity of the amino groups was observed.

The sums of the bond angles around the N12 and N13 atoms, ΣN12 and ΣN13, are given. In the calculations HF/3-21G, HF/6-31G, B3LYP/3-21G, and B3LYP/6-31G, the two sums are 360°, while in the rest of the calculations with other basis sets these sums differ from 360°. In the case of perfect sp^3 hybridisation this sum is 328.5°, and for sp^2 it is 360°.

Ab initio calculations at the HF/3-21G and HF/6-31G levels provide reasonably good geometries. Compared to the experimental data [14] the calculated geometries obtained at these levels had small average errors, in bond lengths (−0.008 Å, −0.006 Å) and in bond angles (0.17°, 0.16°), with a standard deviation of 0.008 and 0.007 Å in bond lengths and 0.93 and 0.84° in bond angles. The geometrical parameters are not necessarily improved by increasing the basis set size and incorporating the electron correlation effect, unless the basis set approaches completeness and correlation is treated far beyond MP2.

The minimal basis set STO-3G provides results, which are inconsistent with experimental data, and with the results from calculations with more flexible basis sets. Thus our results refer to calculations at the higher levels mentioned above. In general, HF gave shorter bond lengths compared to MP2 and B3LYP. Compared to experimental data, HF gave shorter bond lengths than those observed in the X-ray structure, whereas those of B3LYP were longer. The MP2 calculations with the basis sets 6-31G*, 6-31G**, 6-311G* and 6-311G** gave approximately the same bond lengths as the B3LYP/6-31G* calculations.

With the exception of the minimal basis set STO-3G, the bond angles were quite near the X-ray values. Tendencies and values of bond angles were practically equal for all basis sets and levels of theory, only the N10–C11–N12 and N12–C11–N13 angles presented differences. The bond angle criterion, which has been related to hybridisation and has been used considerably [26], varied between the different basis sets.

As can be seen in Tables 1 and 2 the average errors and standard deviations in bond lengths and bond angles between calculated and experimental [14] values are quite small and of the same order of magnitude as the differences between the two experimental geometries as discussed above. Furthermore the calculated values cluster around the experimental values with HF off at the short side in bond lengths as much as the MP2 and B3LYP calculations are off on the long side. And we do not pretend to address the problem the planarity or non-planarity of the amino groups in this work. With all this in mind we decided to use HF/3-21G and HF/6-31G in the further analyses of the conformer **1** and of the protonated and radical species: bond lengths, angles, bond order, NBO, and thermochemistry.

In the guanidine group, the imine bond, N10–C11, is clearly shorter (1.303 Å, HF/3-21G; 1.358 Å,

Table 1
Calculated total Energies, E_{tot} (a.u.), Zero-Point Energies, ZPE (kcal/mol), and structural parameters at HF level for **1**

	HF							X-ray[a]
	STO-3G	3-21G	6-31G	6-31G*	6-31G**	6-311G*	6-311G**	
E_{tot}	−573.1664	−577.2260	−580.2273	−580.4684	−580.4959	580.5883	−580.6108	
Bond lengths								
N1–C2	1.396	1.374	1.369	1.360	1.361	1.360	1.360	1.371
N1–C8	1.399	1.386	1.387	1.379	1.379	1.379	1.379	1.387
N3–C2	1.325	1.316	1.317	1.301	1.301	1.299	1.299	1.340
N3–C9	1.422	1.396	1.396	1.383	1.383	1.383	1.383	1.406
C4–C5	1.374	1.382	1.386	1.384	1.384	1.384	1.383	1.386
C4–C9	1.402	1.382	1.386	1.388	1.387	1.387	1.386	1.394
C5–C6	1.407	1.394	1.398	1.396	1.395	1.395	1.395	1.394
C6–C7	1.375	1.384	1.387	1.384	1.385	1.384	1.384	1.390
C7–C8	1.397	1.379	1.384	1.383	1.383	1.383	1.382	1.387
C8–C9	1.399	1.401	1.400	1.397	1.397	1.396	1.396	1.401
C2–N10	1.426	1.351	1.358	1.362	1.361	1.361	1.361	1.372
N10–C11	1.304	1.303	1.306	1.289	1.291	1.288	1.289	1.320
C11–N12	1.407	1.341	1.345	1.345	1.343	1.345	1.344	1.349
C11–N13	1.430	1.351	1.353	1.367	1.364	1.368	1.366	1.358
N1–H	1.019	0.994	0.989	0.993	0.991	0.990	0.991	
N12–H121	1.032	1.011	1.002	1.001	1.000	0.996	1.000	
N12–H122	1.024	0.995	0.990	0.994	0.992	0.991	0.992	
N13–H131	1.027	0.996	0.990	0.996	0.994	0.993	0.994	
N13–H132	1.028	0.994	0.989	0.996	0.994	0.993	0.995	
N3−-H121	1.832	1.902	1.977	2.000	1.988	2.012	1.996	2.050
Average error[b]	0.015	−0.008	−0.006	−0.010	−0.010	−0.010	−0.010	
Standard deviation	0.028	0.008	0.007	0.013	0.012	0.013	0.013	
Bond angles								
∠N1–C2–N3	112.64	111.26	111.54	112.47	112.33	112.50	112.49	112.07
∠N1–C2–N10	117.43	119.23	118.75	117.18	117.27	117.11	117.16	117.42
∠N1–C8–C7	132.70	133.03	132.92	133.09	133.04	133.08	133.04	131.87
∠N1–C8–C9	105.06	104.99	104.92	104.37	104.41	104.39	104.42	105.01
∠C2–N1–C8	107.12	108.00	107.95	107.61	107.65	107.55	107.54	107.96
∠C2–N3–C9	104.50	106.47	106.22	105.55	105.61	105.59	105.60	104.65
∠C2–N10–C11	116.11	121.48	121.95	120.99	120.74	121.07	120.99	120.54
∠N3–C2–N10	129.92	129.51	129.71	130.35	130.40	130.39	130.35	130.49
∠N3–C9–C4	129.67	130.76	130.46	130.20	130.24	130.25	130.26	130.59
∠N3–C9–C8	110.69	109.29	109.37	110.01	110.00	109.97	109.94	110.29
∠C4–C5–C6	121.31	121.09	121.19	121.27	121.29	121.25	121.28	122.26
∠C4–C9–C8	119.65	119.95	120.17	119.79	119.76	119.78	119.80	119.11
∠C5–C4–C9	118.27	118.43	118.12	118.21	118.23	118.25	118.21	117.98
∠C5–C6–C7	121.45	121.06	121.19	121.16	121.12	121.12	121.14	120.38
∠C6–C7–C8	117.08	117.48	117.17	117.02	117.05	117.08	117.04	117.14
∠C7–C8–C9	122.24	121.98	122.16	122.54	122.55	122.53	122.54	123.11
∠N10–C11–N12	128.14	124.85	125.37	127.20	126.47	127.29	127.11	125.39
∠N10–C11–N13	117.64	117.24	117.04	117.48	116.83	117.44	117.41	116.76
∠N12–C11–N13	114.22	117.91	117.58	115.31	116.71	115.27	115.48	117.71
Average error[b]	−0.26	0.17	0.16	0.06	0.05	0.06	0.06	
Standard deviation	1.58	0.93	0.84	0.92	0.85	0.94	0.89	
Sigma angle								
∠ΣN12	338	360	360	353	355	353	353	
∠ΣN13	331	360	360	345	347	345	345	

Bond lengths in Angström, bond angles in degrees, sigma angles in degrees.

[a] Ref. [14].

Table 2
Calculated total Energies E_{tot} (a.u.), Zero-Point Energies ZPE (kcal/mol), and structural parameters at MP2 and B3LYP levels for **1**

	MP2				B3LYP		
	6-31G*	6-31G**	6-311G*	6-311G**	3-21G	6-31G	6-31G*
E_{tot}	−580.4621	−580.4923	−582.5123	−582.5832	−580.8411	−583.8953	−584.0624
Bond lengths							
N1–C2	1.377	1.377	1.376	1.376	1.394	1.390	1.381
N1–C8	1.377	1.376	1.375	1.375	1.390	1.394	1.383
N3–C2	1.334	1.334	1.332	1.332	1.352	1.350	1.331
N3–C9	1.386	1.386	1.384	1.384	1.398	1.401	1.386
C4–C5	1.391	1.391	1.393	1.393	1.395	1.398	1.394
C4–C9	1.401	1.401	1.403	1.403	1.395	1.399	1.399
C5–C6	1.411	1.410	1.413	1.412	1.406	1.410	1.406
C6–C7	1.392	1.392	1.394	1.394	1.397	1.400	1.396
C7–C8	1.398	1.398	1.400	1.399	1.391	1.395	1.393
C8–C9	1.417	1.417	1.419	1.419	1.426	1.424	1.419
C2–N10	1.375	1.374	1.373	1.373	1.353	1.363	1.364
N10–C11	1.307	1.307	1.305	1.304	1.329	1.328	1.310
C11–N12	1.363	1.362	1.363	1.363	1.353	1.359	1.361
C11–N13	1.386	1.385	1.384	1.386	1.365	1.369	1.383
N1–H	1.012	1.007	1.008	1.009	1.011	1.006	1.009
N12–H121	1.024	1.083	1.017	1.021	1.046	1.029	1.025
N12–H122	1.012	1.083	1.007	1.009	1.012	1.007	1.011
N13–H131	1.014	1.083	1.008	1.011	1.011	1.006	1.012
N13–H132	1.014	1.083	1.009	1.011	1.010	1.005	1.013
N3···H121	1.925	1.020	1.938	1.904	1.761	1.858	1.910
Average error[a]	0.004	0.004	0.004	0.004	0.007	0.009	0.004
Standard deviation	0.013	0.013	0.014	0.014	0.011	0.008	0.012
Bond angles							
∠N1–C2–N3	111.90	111.90	112.09	112.06	110.59	111.07	111.68
∠N1–C2–N10	117.30	117.39	117.08	117.17	120.01	119.38	118.00
∠N1–C8–C7	133.06	133.03	133.08	133.06	133.10	132.92	133.09
∠N1–C8–C9	104.41	104.43	104.39	104.40	105.03	104.98	104.45
∠C2–N1–C8	108.11	108.11	108.02	108.03	108.40	108.20	107.99
∠C2–N3–C9	105.03	105.03	104.96	104.99	106.26	105.96	105.61
∠C2–N10–C11	119.11	118.85	119.21	118.88	119.32	120.23	119.88
∠N3–C2–N10	130.80	130.71	130.83	130.76	129.39	129.56	130.32
∠N3–C9–C4	129.61	129.64	129.70	129.72	130.65	130.30	130.15
∠N3–C9–C8	110.54	110.53	110.53	110.52	109.71	109.80	110.27
∠C4–C5–C6	121.44	121.45	121.41	121.42	121.18	121.29	121.39
∠C4–C9–C8	119.84	119.82	119.77	119.75	119.64	119.90	119.58
∠C5–C4–C9	117.96	117.96	118.06	118.05	118.61	118.22	118.27
∠C5–C6–C7	121.61	121.61	121.55	121.55	121.11	121.29	121.29
∠C6–C7–C8	116.62	116.62	116.68	116.68	117.60	117.19	117.01
∠C7–C8–C9	122.53	122.54	122.53	122.54	121.87	122.10	122.46
∠N10–C11–N12	127.18	127.02	127.33	127.10	124.10	124.59	126.44
∠N10–C11–N13	117.71	117.73	117.67	117.78	116.71	116.93	117.60
∠N12–C11–N13	115.11	115.25	115.00	115.12	119.19	118.47	115.95
Average error[a]	−0.04	−0.06	−0.04	−0.06	0.09	0.09	0.04
Standard deviation	1.03	1.02	1.05	1.03	1.16	0.87	0.78
Sigma angle							
∠ΣN12	348	349	347	347	360	360	351
∠ΣN13	338	339	339	338	360	360	342

Bond lengths in Angström, bond angles in degrees, sigma angles in degrees.

[a] Error = calculated − experimental.

HF/6-31G) than the amino bonds, C11–N12 and C11–N13, (1.341 and 1.351 Å, HF/3-21G; 1.345 and 1.353 Å, HF/6-31G), and the C2–N10 bond (1.351 Å, HF/3-21G; 1.359 Å, HF/6-31G).

At the HF/3-21G and HF/6-31G levels, the N12–H121 bond is longer than the N12–H122 bond by 0.016 and 0.012 Å. These differences in bond lengths may be due to an intra-molecular hydrogen bond, H121···N3, (X-ray: 2.050 Å [14], HF/3-21G: 1.902 Å, HF/6-31G: 1.977 Å).

3.1.2. Bond order

The calculated bond orders [27] for conformer **1** listed in Table 3 show similar trends at the HF/3-21G and HF/6-31G levels. The HF/6-31G calculation gave the following results in the guanidine fragment: the C2–N10 bond order was 1.187 and the N10–C11 bond order was 1.521, while for the bonds C11–N12 and C11–N13 the values were 1.020 and 0.953, respectively. This shows the conjugation between the ring π-system and the N10–C11 bond via the C2–N10 bond, while the other C11–Nnn′ bonds have essentially single bond character. This is congruent with our calculated bond lengths, where the imine bond was shorter than the amino bonds. On the other hand, the N12–H121 bond (0.717) is weakened compared to the N12–H122 bond (0.838) due to the intramolecular hydrogen bond, H121···N3. In the benzimidazole group, the six bonds in the benzene ring have bond orders in the range 1.333–1.477.

3.1.3. Charge analysis

The charge distributions calculated by the Mulliken [28] and NBO [18] methods for the equilibrium geometry of **1** are given in Table 4. Both methods predict the same tendencies, assigning positive partial charges of similar magnitudes on the hydrogen atoms, while there were greater variations between the methods in the magnitudes of the partial charges on the carbon and nitrogen atoms. Both methods predict, that the hydrogen atoms bonded to N12 and N13 are acidic, while the nitrogen atoms N3 and N10 are the basic sites. The dipole moment of **1** is calculated to be 4.1 Debye at the RHF/6-31G level.

3.1.4. NBO analysis

It is important to recall, that in the NBO analysis, the electronic wavefunction is interpreted in terms of a set of highly occupied Lewis and a set of weakly occupied non-Lewis localized orbitals [18b]. Delocalisation effects can be identified from the presence of off-diagonal elements between these two sets in the Fock-matrix. These delocalisation interactions, $E^{(2)}$, are estimated by second-order perturbation theory.

The stabilization energies are given in Table 5, estimated by the interaction between the ‘filled’ Lewis-type NBOs and the ‘empty’ non-Lewis NBOs. The results indicate the presence of interactions, which lead to a small change in the occupancy from the localized NBOs of the idealized Lewis structure into the empty non-Lewis orbitals. This is referred to as the delocalisation corrections to the natural Lewis structure [18c]. The set of 46 strongly occupied NBOs have almost 98% of the electrons. The most important delocalisation sites are in the π system, and in the lone pairs (n) of the nitrogens. The σ system shows some contribution to the delocalisation. The $n_{N12} \rightarrow \pi^*_{N10-C11}$ interaction is the most important contribution to a strong resonant system in **1** (100.3 kcal/mol, HF/6-31G). Another contribution to the delocalisation corresponds to a donor–acceptor interaction, the N3 nitrogen lone pair orbital of σ-type to the remote N12–H121σ* antibonding orbital, as a consequence of the short intramolecular N12–H121···N3 hydrogen bond (Table 1), which leads to the formation of a six-membered ring.

The percentage of p-character [18d] in each NBO natural atomic hybrid orbital is presented in Table 6. An ideal sp^2 hybrid has a p-character of 66.7%. The results for the σ bonds show variations around this value. In the benzene ring, the σ_{CC} benzene bonds are formed from carbon hybrid orbitals with a p-character slightly lower on C4, C5, C6 and C7. On C8 and C9, the hybrids in the C7–C8 and C4–C9 bonds the p-character is reduced to 60–61% (HF/6-31G). In the imidazole ring, the hybrids on C8 and C9 demonstrate a strong deviation in the opposite direction to 73–71%. The in-ring nitrogen hybrids have a slight reduction similar to what was observed on C4, C5, C6 and C7. In the C–H and N–H bonds, the carbon and nitrogen hybrids show increase to about 70% except for the N12–H121 case, which is involved in the hydrogen bonding to N3. Here the p-character is down to 66.8%. Finally, the σ lone pair on N10 has a strong increase to 72.1%. These results confirm that

Table 3
Calculated bond order p(A–B) at HF level for **1**

	3-21G	6-31G
p(N1–C2)	0.916	0.908
p(N1–C8)	0.735	0.709
p(N3–C2)	1.354	1.364
p(N3–C9)	0.995	1.057
p(C4–C5)	1.443	1.477
p(C4–C9)	1.350	1.397
p(C5–C6)	1.377	1.408
p(C6–C7)	1.437	1.468
p(C7–C8)	1.348	1.391
p(C8–C9)	1.287	1.333
p(C2–N10)	1.102	1.187
p(C10–N11)	1.403	1.521
p(C11–N12)	1.034	1.020
p(C11–N13)	0.949	0.953
p(N1–H)	0.843	0.826
p(C4–H)	0.934	0.930
p(C5–H)	0.942	0.946
p(C6–H)	0.941	0.945
p(C7–H)	0.938	0.932
p(N12–H121)	0.708	0.717
p(N12–H122)	0.852	0.838
p(N13–H131)	0.831	0.819
p(N13–H132)	0.853	0.840
p(N···H121)	0.111	0.080

the standard chemical description of the bonding and hybridisation in 2gb provides a very adequate model.

3.1.5. Molecular electrostatic potential of 1

EPS maps are known to provide useful information about spatial charge distributions in a molecule [33]. We have examined the EPS in the molecular plane of **1** calculated with the HF/6-31G calculated density, which has been depicted in Fig. 7. Large pockets of negative potential can be found in front of the N3 and N10 atoms, while the rest of the areas around the molecule have positive potentials. The $V(r)$ contours drawn in the graphic are in the range ±45 kcal/mol/electron charge.

3.2. Protonated species

3.2.1. Relative energies of 3 and 5

The two structures are predicted to be planar, and **3**, at HF/6-31G, is 5.7 kcal/mol lower in energy than

Table 4
The charge distribution calculated by the Mulliken and Natural Bond Orbital (NBO) methods at HF level for **1**

	3-21G Mulliken	NBO	6-31G Mulliken	NBO
q(N1)	−1.055	−0.678	−1.038	−0.653
q(C2)	1.078	0.735	0.878	0.686
q(N3)	−0.844	−0.687	−0.720	−0.686
q(C4)	−0.224	−0.241	−0.138	−0.233
q(C5)	−0.251	−0.262	−0.219	−0.260
q(C6)	−0.242	−0.251	−0.221	−0.248
q(C7)	−0.223	−0.273	−0.118	−0.269
q(C8)	0.385	0.155	0.339	0.140
q(C9)	0.232	0.135	0.105	0.129
q(N10)	−0.919	−0.779	−0.717	−0.756
q(C11)	1.178	0.840	0.971	0.784
q(N12)	−0.978	−0.931	−0.963	−0.921
q(N13)	−0.958	−0.905	−0.959	−0.899
q(H1)	0.374	0.447	0.392	0.455
q(H4)	0.244	0.245	0.213	0.246
q(H5)	0.230	0.237	0.189	0.239
q(H6)	0.232	0.237	0.189	0.239
q(H7)	0.235	0.240	0.209	0.241
q(H121)	0.442	0.479	0.469	0.488
q(H122)	0.342	0.408	0.368	0.418
q(H131)	0.347	0.435	0.371	0.444
q(H132)	0.376	0.411	0.399	0.419
q(N1H)	−0.681	−0.231	−0.646	−0.198
q($N12H_2$)	−0.195	−0.044	−0.126	−0.016
q($N13H_2$)	−0.235	−0.058	−0.188	−0.036

Table 5
The second-order perturbation energies $E^{(2)}$ (donor → acceptor)

Donor	Type	Acceptor	Type	Energy 3-21G	6-31G
N3–C2	π	C8–C9	π^*	31.3	30.8
N3–C9	σ	C2–N10	σ^*	8.5	10.1
C4–C5	π	C6–C7	π^*	40.8	41.2
C4–C5	π	C8–C9	π^*	36.2	36.7
C6–C7	π	C4–C5	π^*	37.7	36.7
C6–C7	π	C8–C9	π^*	38.3	38.4
C8–C9	π	N3–C2	π^*	17.1	18.7
C8–C9	π	C4–C5	π^*	41.7	41.2
C8–C9	π	C6–C7	π^*	43.00	42.6
N10–C11	π	N3–C2	π^*	57.5	53.7
N1	n	N3–C2	π^*	83.9	83.2
N1	n	C8–C9	π^*	47.7	45.7
N3	n	N1–C2	σ^*	11.1	12.7
N3	n	N12–H	σ^*	22.6	13.9
N10	n	N3–C2	σ^*	15.3	15.9
N10	n	C11–N12	σ^*	18.1	19.7
N10	n	C11–N13	σ^*	9.2	6.5
N12	n	N10–C11	π^*	107.6	100.3
N13	n	N10–C11	π^*	86.4	81.9

Energies (they are included only in the interaction energy that exceeds 5 kcal/mol) in kcal/mol.

Table 6
Percentage of p-character on each natural atomic hybrid of which the natural bond orbital (NBO) is composed, at HF level, on **1**

NBO	Atom	3-21G	6-31G
N1–C2	N1	65.3	65.7
	C2	70.0	69.9
N1–C8	N1	65.3	65.3
	C8	74.14	73.0
N3–C2	N3	63.2	64.3
	C2	64.9	64.7
N3–C9	N3	65.9	65.9
	C9	72.4	71.3
C4–C5	C4	64.7	64.5
	C5	65.0	64.8
C4–C9	C4	66.1	65.8
	C9	60.7	61.4
C5–C6	C5	65.3	65.1
	C6	65.1	64.8
C6–C7	C6	65.3	65.0
	C7	64.4	64.3
C7–C8	C7	66.4	66.1
	C8	59.6	60.2
C8–C9	C8	66.4	67.0
	C9	67.2	67.5
C2–N10	C2	65.2	65.5
	N10	63.4	64.0
N10–C11	N10	61.4	62.0
	C11	64.0	63.9
C11–N12	C11	66.7	66.8
	N12	63.2	63.5
C11–N13	C11	69.3	69.3
	N13	61.1	61.6
N1–H1	N1	69.5	69.1
C4–H4	C4	69.2	69.6
C5–H5	C5	69.6	70.1
C6–H6	C6	69.6	70.2
C7–H7	C7	69.2	69.1
N12–H121	N12	66.9	66.8
N12–H122	N12	70.0	69.8
N13–H131	N13	69.6	69.3
N13–H132	N13	69.4	69.1

5. With the inclusion of the ZPE correction, **3** is more stable than **5** by 6.4 kcal/mol (Table 7).

3.2.2. Geometry

The geometric parameters of **3**, **5** and **6** are presented in Table 7. At the HF/3-21G and HF/6-31G levels, the interatomic distances of **6** are very close to the experimental values. At the HF/3-21G level, in the two species **5** and **6** the bond lengths present similar tendencies. However, the C2–N10 bond is longer in **5** than in **6**. This result is explained from the X-ray structure of **6**, where N10 (protonation site) is involved in hydrogen bonding with an oxygen atom in the acetate molecule, whereas the specie **5** does not present hydrogen bonding in this position.

Protonation may lead to an increase or decrease of the bond distance for an atom bonded to the protonation site [29]. In specie **3** the 'double bond' N3–C2 increased by 0.038 Å and the 'single bond' C9–N3 by 0.014 Å; while in specie **5** the increases in the 'double bond' N10–C11 and the 'single bond' C2–N10 were 0.045 and 0.038 Å, respectively. In both species the increase in bond length was greater in the 'double bond', i.e. this bond is weakened by the protonation. Furthermore, this effect is larger, when the protonation occurs in the guanidine group.

In the doubly protonated specie **4** the increments in bond length were: 'single bond' N3–C9 0.022 Å, 'double bond' N3–C2 0.027 Å, 'single bond' C2–N10 0.025 Å and 'double bond' N10–C11 0.063 Å. And it should be noted, that the increase of these bond lengths is larger in the guanidine group.

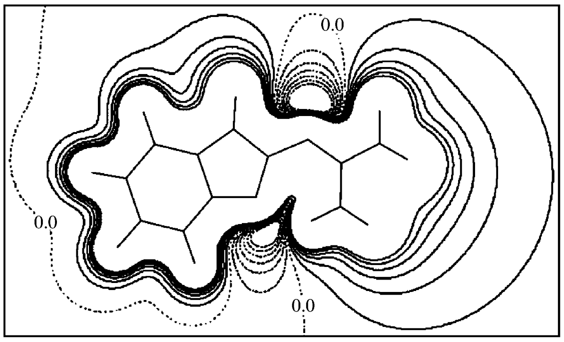

Fig. 7. ESP map of the molecular plane of **1**, calculated at the HF/6-31G level. Each contour level is 7.5 kcal/mol/electroncharge. Positive isopotential lines are solid; negative isopotential lines are dashed.

3.2.3. Charge analysis

Table 8 shows the charge distribution calculated by the NBO and Mulliken methods for the species **3** and **5** at their equilibrium geometries. The two methods assigned positive partial charges of similar

Table 7
Calculated total Energies E_{tot} (a.u.), Zero-Point Energies ZPE (kcal/mol), and structural parameters for **3**, **4**, **5** and **6** at HF level

	3		**4**		**5**		**6**	
	3-21G	6-31G	3-21G	6-31G	3-21G	6-31G	3-21G	X-ray[a]
E_{tot}	−577.6333	−580.6297	−577.8566	−580.8519	−577.6259	−580.6207	−879.4288	
ZPE	127.8492	128.9278	136.527	137.8512	128.2343	129.3813		
Bond lengths								
N1–C2	1.345	1.342	1.327	1.327	1.361	1.359	1.353	1.354
N1–C8	1.398	1.399	1.412	1.410	1.401	1.401	1.386	1.393
N3–C2	1.357	1.355	1.327	1.328	1.289	1.290	1.308	1.317
N3–C9	1.410	1.410	1.422	1.418	1.408	1.405	1.400	1.398
C4–C5	1.384	1.387	1.380	1.383	1.377	1.381	1.379	1.379
C4–C9	1.377	1.381	1.381	1.385	1.384	1.388	1.384	1.386
C5–C6	1.393	1.397	1.400	1.404	1.399	1.403	1.398	1.387
C6–C7	1.383	1.386	1.380	1.383	1.379	1.382	1.380	1.397
C7–C8	1.377	1.382	1.381	1.385	1.382	1.387	1.383	1.385
C8–C9	1.384	1.385	1.379	1.382	1.391	1.393	1.397	1.391
C2–N10	1.309	1.322	1.378	1.383	1.394	1.396	1.380	1.379
N10–C11	1.314	1.320	1.370	1.369	1.353	1.351	1.342	1.349
C11–N12	1.341	1.344	1.312	1.317	1.305	1.311	1.325	1.320
C11–N13	1.329	1.332	1.313	1.317	1.328	1.332	1.320	1.330
N1–H	0.998	0.992	1.003	0.997	0.997	0.991	1.034	
N3–H	0.993	0.988	0.995	0.990				
C4–H	1.070	1.072	1.070	1.071	1.070	1.071	1.070	
C5–H	1.070	1.071	1.070	1.071	1.071	1.071	1.072	
C6–H	1.070	1.071	1.070	1.071	1.071	1.072	1.072	
C7–H	1.070	1.071	1.070	1.071	1.070	1.072	1.071	
N10–H			1.005	0.999	1.000	0.994	1.054	
N12–H121	0.991	0.987	0.993	0.989	1.025	1.011	1.020	
N12–H122	0.999	0.993	1.006	0.999	0.999	0.994	0.997	
N13–H131	0.999	0.993	1.003	0.997	0.999	0.993	1.040	
N13–H132	0.997	0.992	1.004	0.998	0.999	0.994	0.997	
N3···H121					1.797	1.884	1.795	1.837
Bond angles								
∠N1–C2–N3	106.43	106.68	108.94	108.91	113.62	113.77		
∠N1–C2–N10	120.15	119.47	120.33	120.34	121.90	121.62		
∠N1–C8–C7	132.44	132.29	132.04	131.92	132.30	132.22		
∠C2–N3–C9	110.14	110.05	109.25	109.32	105.98	105.79		
∠C2–N10–C11	134.12	133.07	133.21	133.66	124.08	125.03		
∠N3–C2–N10	133.41	133.85	130.73	130.74	124.47	124.61		
∠N3–C9–C4	131.94	131.81	131.69	131.60	130.58	130.29		
∠N3–C9–C8	106.16	106.13	106.04	106.03	108.65	108.83		
∠C4–C5–C6	121.23	121.38	121.63	121.78	121.23	121.33		
∠C5–C6–C7	121.35	121.51	121.66	121.81	121.52	121.64		
∠C6–C7–C8	117.11	116.76	116.28	115.96	116.77	116.49		
∠C7–C8–C9	121.45	121.65	122.00	122.18	122.12	122.31		
∠C8–N1–C2	111.16	111.08	109.81	109.84	106.16	106.15		
∠C8–C9–C4	121.90	122.06	122.28	122.37	120.78	120.88		
∠C9–C4–C5	116.96	116.64	116.16	115.89	117.58	117.35		
∠C9–C8–N1	106.11	106.06	105.96	105.90	105.59	105.47		
∠N10–C11–N12	127.04	127.42	123.31	123.57	119.96	120.55		
∠N10–C11–N13	115.80	115.55	116.29	116.44	117.88	118.02		

(*continued on next page*)

Table 7 (*continued*)

	3		**4**		**5**		**6**	
	3-21G	6-31G	3-21G	6-31G	3-21G	6-31G	3-21G	X-ray[a]
∠N12–C11–N13	117.16	117.04	120.40	120.00	122.16	121.43		
Sigma angle								
∠ΣN12	360	360	360	360	360	360		
∠ΣN13	360	360	360	360	360	360		

Bond lengths in Angström, bond angles in degrees, sigma angles in degrees.
[a] Ref. [7].

magnitudes to the hydrogen atoms, while the charges on the carbon and nitrogen atoms differed more between the two methods, though the overall trends were the same. Both methods predict that, when the protonation of **1** occurs on N3, specie **3**, the electron density diminished slightly on the protonated atom N3 and to a lesser extent on the neighbouring atoms C9 and C2; while the atoms further from the protonation site were practically non-altered with the exception of N12, where the reduction in the electron density was similar to what was observed on N3. This can be explained by the breaking of the intramolecular hydrogen bond upon protonation of N3. When the protonation occurs N10, specie **5**, the reduction of the electron density on the protonated atom and its immediate neighbours is somewhat larger than in the previous case, and second neighbours are also affected to some extent (reduction). In the bi-protonated specie **4**, the effect is essentially the sum of the effects in the mono-protonated forms.

3.2.4. NBO analysis

The NBO charge transfer for **3** and **5** is reported in Table 9. The set of 46 strongly occupied NBOs account for almost 97% of the total electron population. Several strong donor–acceptor interactions are observed, the principal delocalisation sites are in the π system and the nitrogen lone pairs (n) of the cationic species. The donor–acceptor interactions in the benzene fragment are the same as those in **1**. The results differ in the absolute values but present similar tendencies. The donor–acceptor contributions in the guanidine group are different from those observed in **1**. The specie **3** presents a strong donor–acceptor interaction between n_{N1} - and π^*_{C2-N10} with an energy of 120.3 kcal/mol at the HF/6-31G level. We will use this calculation for the discussion in this section. The results were very similar in the HF/3-21G calculation. This interaction does not exist in **1** or **5**. There are two important interactions, which are present in **3** but not in **1** or **5**, the interactions are $\pi_{C2-N10} \rightarrow 1/2n_{C11}$ 120.6 kcal/mol and $n_{N3} \rightarrow \sigma^*_{C2-N10}$ 110.9 kcal/mol. When an unpaired electron occupies a lone pair orbital n, it is termed a half lone pair, 1/2n. The results for **3** and **5** showed that strongest interactions were $\pi_{N12} \rightarrow 1/2n_{C11}$ 130.6 kcal/mol, and $\pi_{N13} \rightarrow 1/2n_{C11}$ 153.2 kcal/mol. In **5** the strongest interactions were $\pi_{N12} \rightarrow 1/2n_{C11}$ 208.5 kcal/mol, and $\pi_{N13} \rightarrow 1/2n_{C11}$ 147.2 kcal/mol.

Other important interactions specific to the protonated forms, which were strong in **3** and weak in **5**, were the $\pi_{C2-N10} \rightarrow 1/2n_{N11}$ 120.6 kcal/mol, and $n_{N3} \rightarrow \sigma^*_{C2-N10}$ 110.9 kcal/mol.

3.3. Thermochemical analysis

A thermochemical analysis was performed and the results are shown in Table 10. The energy difference between the protonated specie and the neutral molecule, calculated at their equilibrium structures, gives the protonation energy ($\Delta E_p = E_{ion}-E_{neutral}$). In several works, these protonation energies have been linearly related to the experimental proton affinities in series of related molecules [30]. Our calculated energy differences between the mono protonated species and **1**, are not quantitatively relevant, but the comparison between the two competing protonation processes is qualitatively significant. At the two theory levels

Table 8
The charge distribution calculated by the Mulliken and Natural Bond Order (NBO) methods for protonated species at HF levels

	3				**4**				**5**				**6**	
	3-21G		6-31G		3-21G		6-31G		3-21G		6-31G		3-21G	
	Mulliken	NBO	Mulliken	NBO	Mulliken	NBO	Mulliken	NBO	Mulliken	NBO	Mulliken	NBO	Mulliken	NBO
q(N1)	−1.042	−0.651	−1.009	−0.611	−1.033	−0.630	−1.015	−0.591	−1.047	−0.678	−1.043	−0.655	−1.103	−0.698
q(C2)	1.301	0.855	1.107	0.791	1.427	0.851	1.343	0.780	1.208	0.726	1.079	0.665	1.187	0.743
q(N3)	−1.049	−0.676	−1.039	−0.649	−1.039	−0.635	−1.019	−0.601	−0.828	−0.628	−0.704	−0.619	−0.858	−0.678
q(C4)	−0.204	−0.250	−0.103	−0.246	−0.191	−0.241	−0.079	−0.238	−0.202	−0.219	−0.104	−0.213	−0.219	−0.237
q(C5)	−0.228	−0.223	−0.207	−0.219	−0.210	−0.190	−0.195	−0.185	−0.241	−0.241	−0.215	−0.239	−0.250	−0.261
q(C6)	−0.228	−0.219	−0.205	−0.215	−0.212	−0.189	−0.195	−0.185	−0.223	−0.213	−0.206	−0.211	−0.241	−0.246
q(C7)	−0.195	−0.246	−0.095	−0.241	−0.183	−0.236	−0.071	−0.233	−0.215	−0.265	−0.104	−0.262	−0.217	−0.258
q(C8)	0.368	0.157	0.308	0.142	0.349	0.151	0.283	0.138	0.375	0.161	0.323	0.147	0.377	0.160
q(C9)	0.343	0.153	0.278	0.139	0.331	0.149	0.261	0.137	0.224	0.117	0.095	0.110	0.229	0.125
q(N10)	−0.958	−0.777	−0.724	−0.754	−1.117	−0.732	−1.088	−0.690	−1.099	−0.730	−1.048	−0.687	−1.167	−0.780
q(C11)	1.245	0.877	1.030	0.814	1.411	0.919	1.272	0.849	1.376	0.905	1.217	0.838	1.324	0.893
q(N12)	−0.945	−0.893	−0.931	−0.886	−0.942	−0.862	−0.911	−0.838	−0.967	−0.885	−0.923	−0.858	−0.986	−0.917
q(N13)	−0.922	−0.874	−0.916	−0.856	−0.926	−0.863	−0.917	−0.837	−0.954	−0.889	−0.947	−0.872	−1.019	−0.921
q(H1)	0.420	0.480	0.438	0.484	0.442	0.494	0.460	0.493	0.393	0.459	0.411	0.463	−0.692	−0.779
q(H3)	0.392	0.449	0.414	0.454	0.428	0.473	0.447	0.474						
q(H4)	0.276	0.262	0.250	0.262	0.309	0.282	0.284	0.280	0.276	0.262	0.246	0.262	0.244	0.245
q(H5)	0.284	0.266	0.242	0.266	0.325	0.288	0.282	0.287	0.273	0.260	0.231	0.260	0.234	0.239
q(H6)	0.285	0.266	0.243	0.266	0.326	0.289	0.283	0.288	0.275	0.260	0.232	0.260	0.237	0.240
q(H7)	0.284	0.267	0.258	0.267	0.315	0.285	0.290	0.284	0.269	0.259	0.242	0.258	0.261	0.253
q(H10)					0.442	0.486	0.461	0.483	0.406	0.461	0.427	0.462	0.485	0.501
q(H121)	0.377	0.427	0.401	0.431	0.416	0.455	0.437	0.455	0.488	0.508	0.513	0.514	0.463	0.492
q(H122)	0.397	0.448	0.420	0.452	0.449	0.491	0.469	0.488	0.400	0.454	0.422	0.456	0.359	0.422
q(H131)	0.413	0.463	0.433	0.467	0.437	0.479	0.456	0.477	0.404	0.454	0.426	0.456	0.464	0.486
q(H132)	0.387	0.440	0.407	0.442	0.445	0.488	0.464	0.486	0.409	0.461	0.431	0.462	0.350	0.416
q(O16)													−0.815	−0.860
q(O17)													−0.710	−0.749
q(O18)													−0.809	−0.960
q(C14)													−0.692	−0.779
q(C15)													0.893	0.938
q(H141)													0.237	0.247
q(H142)													0.222	0.240
q(H143)													0.230	0.245
q(H181)													0.459	0.518
q(H182)													0.369	0.447

Table 9
The second-order perturbation energies $E^{(2)}$ (donor → acceptor) at HF level for protonated species **3** and **5**

Donor	Type	Acceptor	Type	**3**		**5**	
				3-21G	6-31G	3-21G	6-31G
C2–N10	π	C11	n	119.3	120.6		
N3–C2	π	C8–C9	π*			22.5	22.8
N3–C9	σ	C2–N10	σ*	6.5	7.9	10.6	12.3
C4–C5	π	C6–C7	π*	40.4	40.3	41.3	41.8
C4–C5	π	C8–C9	π*	45.4	45.7	39.5	40.0
C6–C7	π	C4–C5	π*	40.9	40.8	35.2	35.1
C6–C7	π	C8–C9	π*	46.5	47.0	43.5	43.8
C8–C9	σ	N1–H	σ*	3.3	4.2	3.6	4.6
C8–C9	σ	N3–H	σ*	3.0	4.0		
C8–C9	π	N3–C2	π*			21.9	24.6
C8–C9	π	C4–C5	π*	37.3	37.0	35.5	35.2
C8–C9	π	C6–C7	π*	35.7	35.3	33.9	33.9
N10–C11	σ	C2–N10	σ*	4.5	2.8	3.4	2.8
N1	n	N3–C2	π*			91.0	88.4
N1	n	C8–C9	π*	37.3	42.2	42.1	40.6
N1	n	C2–N10	π*	120.1	120.3		
N3	n	N1–C2	σ*			12.1	13.9
N3	n	C2–N10	π*	112.1	110.9		
N3	n	C8–C9	π*	37.3	36.1		
N3	n	N12–H121	σ*			32.8	19.6
N10	n	N1–C2	σ*	12.1	8.4		
N10	n	N3–C2	σ*	26.2	25.6	53.5	51.3
N10	n	C11–N12	σ*	20.9	21.5		
N10	n	C11–C13	σ*	11.0	7.8		
N10	n	C11	n			135.0	134.3
N12	n	C11	n	141.7	130.6	231.3	208.5
N13	n	C11	n	165.3	153.2	159.0	147.2
C11	n*	C2–N10	π*	77.0	80.7		

Energies (they are included only in the interaction energy that exceeds 5 kcal/mol) in kcal/mol.

used, the results were similar. The protonation energy calculated for the process 1 → 3 was 243.6 kcal/mol (HF/6-31G + ZPE), and resulted 6.1 kcal/mol higher than for 1 → 5, Fig. 4.

Formally, the enthalpy of reaction for the formation of the protonated specie from its neutral contra-part is defined in terms of a quantity called the proton affinity, PA. It is the negative of

Table 10
Calculated thermodynamic parameters of **1**, **3** and **5** and their protonated forms in the gaseous phase and HOMO

Compound	**1**		**3**		**4**		**5**	
	3-21G	6-31G	3-21G	6-31G	3-21G	6-31G	3-21G	6-31G
ΔH_f	−362,089.7	−364,117.2	−362,336.6	−364,215.7	−362,468.4	−364,346.6	−362,331.3	−364,209.3
ΔG_f	−632,118.1	−364,000.5	−362,364.7	−364,243.9	−362,495.6	−364,374.0	−362,359.9	−364,238.2
ΔE_p			255.6	252.5	395.7	392.0	251.0	246.9
$\Delta E_{p(ZPE)}$			246.7	243.6	382.1	380.0	241.7	237.5
PA			560.5	412.1	1 005.8	856.6	555.2	405.7
GB			−560.1	−557.1	−1004.6	−1000.6	−555.4	−551.2

ΔH, ΔS and ΔG are in kcal/mol and HOMO in eV.

Table 11
Calculated total energies E_{tot} (a.u.), and structural parameters for radical species at HF/3-21G level

	7
E_{tot}	−576.5964
Bond lengths	
N1–C2	1.481
N1–C8	1.346
N3–C2	1.310
N3–C9	1.402
C4–C5	1.407
C4–C9	1.380
C5–C6	1.410
C6–C7	1.392
C7–C8	1.409
C8–C9	1.433
C2–N10	1.329
N10–C11	1.315
C11–N12	1.337
C11–N13	1.344
N1–H	
C4–H	1.070
C5–H	1.072
C6–H	1.072
C7–H	1.070
N12–H121	1.011
N12–H122	0.996
N13–H131	0.998
N13–H132	0.994
N3···H121	1.901
Bond angles	
N1–C2–N3	112.67
N1–C2–N10	117.93
N1–C8–C7	129.35
C2–N3–C9	106.40
C2–N10–C11	121.91
N3–C2–N10	129.40
N3–C9–C4	131.03
N3–C9–C8	107.89
C4–C5–C6	121.64
C5–C6–C7	120.99
C6–C7–C8	117.83
C7–C8–C9	120.68
C8–N1–C2	103.06
C8–C9–C4	121.08
C9–C4–C5	117.79
C9–C8–N1	109.97
N10–C11–N12	124.55
N10–C11–N13	116.63
N12–C11–N13	118.82
Sigma angle	
ΣN12	360.00
ΣN13	359.99

Bond lengths in Angström, bond angles in degrees, sigma angles in degrees.

Table 12
The charge distribution calculated by the Mulliken and Natural Bond Orbital (NBO) methods at HF/3-21G level for **7**

	Mulliken	NBO
q(N1)	−0.603	−0.122
q(C2)	0.967	0.648
q(N3)	−0.823	−0.663
q(C4)	−0.234	−0.237
q(C5)	−0.250	−0.274
q(C6)	−0.237	−0.240
q(C7)	−0.228	−0.278
q(C8)	0.312	0.086
q(C9)	0.280	0.118
q(N10)	−0.908	−0.770
q(C11)	1.177	0.841
q(N12)	−0.977	−0.925
q(N13)	−0.957	−0.901
q(H1)		
q(H4)	0.249	0.250
q(H5)	0.230	0.238
q(H6)	0.235	0.240
q(H7)	0.244	0.246
q(H121)	0.443	0.479
q(H122)	0.347	0.412
q(H131)	0.383	0.441
q(H132)	0.350	0.413

the enthalpy change of the hypothetical protonation reaction: $\Delta H_{reac} = -PA$, for the reactions:

$$\text{Conformer I} + H^+ \rightarrow \text{cat-H3} \quad (1)$$

or

$$\text{Conformer I} + H^+\text{cat-H10} \quad (2)$$

The PA values obtained were 412.1 kcal/mol for reaction (1) and 405.7 kcal/mol for reaction (2) at the HF/6-31G level. Both the HF/3-21G and HF/6-31G calculations predict that the specie **3** is the strongest base towards a proton.

The basicity, $\delta\Delta G_{(B)}$, of a given base B, can be defined as the standard free energy change for protonation process. The $\delta\Delta G_{(B)}$ of the reactions (1) and (2) it can be expressed as in Eq. (3).

$$\delta\Delta G_{(B)} = [\Delta G_{(BH^+)}] - [\Delta G_{(B)} + \Delta G_{(H^+)}] \quad (3)$$

In this equation, B is the neutral specie (**1**) and BH^+ is the protonated specie (**3**, **4**, or **5**) of the base B. The Gibbs energy change associated with

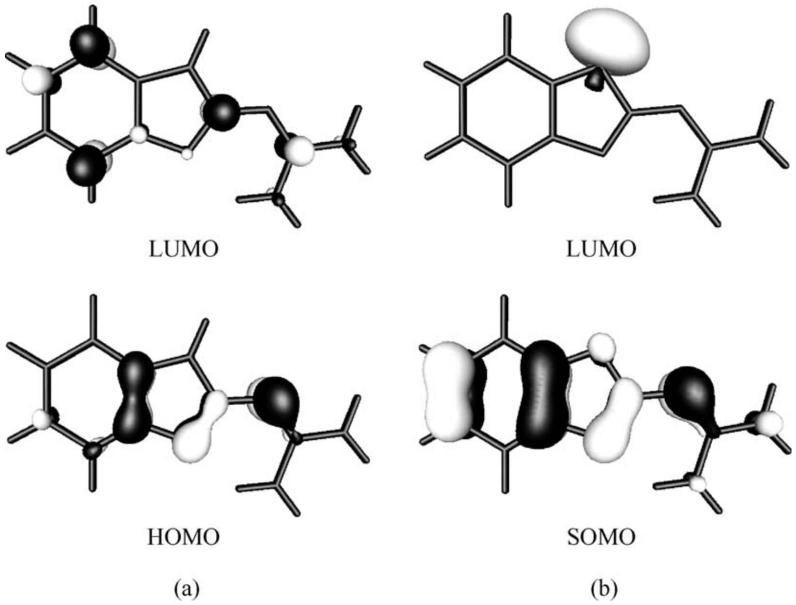

Fig. 8. Frontier orbitals. (a) HOMO and LUMO for **1**. (b) SOMO and LUMO for **7**.

the protonation reaction is called the gas phase basicity, GB, of the molecule. For the reactions (1) and (2), the calculated (HF/6-31G) gas phase basicity of **1** was −557.1 kcal/mol (reaction (1)) and −551.2 kcal/mol (reaction (2)), respectively. The double protonated specie **4** resulted to have roughly twice the basicity of a mono-protonated specie.

In a paper by Del Bene [31], the correlation between the experimental ionisation potentials and protonation energies of bases in a series of molecules was published, and it was suggested that the ionisation potential is a measure of the donor ability and consequently the PA of a base. And several authors have suggested the correlation between the n orbital energies (the n ionisation potentials as approximated by Koopmans' theorem) and the relative proton affinities of the diazines [31] and imidazole [32].

3.4. Radical formation

3.4.1. Geometry

The formation of a radical was studied by analysing a probable electronic structure, **7** (Fig. 5). The optimised structural parameters and total energies are given in Table 11. The UHF/3-21G level predicts a planar geometry for **7**. The bond lengths values for **7** are close to those of **1**, with the exception of the N1–C2 bond (0.17 Å). The sums ΣN12 and ΣN13 are 360°. The bond angles of **7** do not present significant variations with respect to **1**.

3.4.2. Charge analysis

Table 12 shows the charge distributions calculated by the NBO and Mulliken methods for the equilibrium geometry of **7**. The two methods predict the same tendency but differ in the absolute values. When the electron density of the radical specie **7** is compared to that of **1** a considerable decrement on N1 (0.555, NBO) is observed. This is the site where the hydrogen atom was extracted; the corresponding charge is mainly relocated to the nitrogen atoms. The species **7** and **1** are isoelectronic.

3.4.3. Frontier molecular orbitals (HOMO and SOMO) of *1* and *7*

Fig. 8 shows the frontier molecular orbitals of **1** and **7**. The HOMO of **1** was localized in the C8–C9, C2–N3 and N10–C11 bonds and with an orbital energy of −7.25 eV. On the other hand, the SOMO (singled occupied molecular orbital) of **7** was situated in the C5–C6, C8–C9, C2–N3, N10–C11 bonds and on the N1 atom, and to a minor extent on the N12, N13 atoms. The SOMO had an orbital energy of −7.29 eV. The LUMO in **1** had π symmetry with an orbital energy of 3.89 eV, while the LUMO in **7** was a σ orbital with some lone pair character on N1 and its energy was 1.17 eV. The characteristics of the SOMO imply that a delocalised radical free is formed, which had been proposed based on the observed EPR spectra [15].

4. Conclusions

We have investigated the molecular structure of 2gb by using HF, MP2 and DFT calculations and compared these with experimental data to assess the accuracy of the theoretical methods. According to our results a modest ab initio theory such as at the HF/3-21G or HF/6-31G levels appears to provide reasonably good geometries, and increasing the basis set size and incorporation of some electron correlation (MP2) does not necessarily lead to better geometrical parameters.

An important structural characteristic of 2gb is the intramolecular hydrogen bond N3···H121. This hydrogen bond plays an important role in the stabilization of the lowest energy isomer, in which a pseudo six ring is formed between the imidazole and guanidine groups. The hydrogen bond provides a weak direct interaction between the imidazole N3 (its lone pair) and the atoms localised in the guanidine fragment.

Based on the NBO analysis these calculations showed that, the structure and properties of 2gb can be adequately discussed in the standard organic chemistry framework of atomic hybridisation.

The charge distribution calculations confirmed that, the nitrogen atoms N3 and N10 due to their σ lone pairs are the basic sites in the specie **1**. In contrast, in the N3 atom the σ lone pair is occupied in the hydrogen bond with the guanidine group. With respect to the basicity of the different possible species, the thermochemical analysis showed that the specie **3** is the strongest base towards a proton in the gas phase. It permits us to predict that, the N3 atom will be the site for electrophilic attack.

In the 2gb molecule a free radical was formed, when the covalent bond N1–H1 was broken by homolysis. At the UHF/3-21G level the SOMO frontier molecular showed that the unpaired electron is delocalised in π system, mainly in the benzimidazole group.

Acknowledgements

The GAUSSIAN calculations were carried out on the Cray Origin2000 (Berenice8) of DGSCA-UNAM (Dirección General de Servicios de Computo Académico). We acknowledge DGPA-UNAM (Grant IN-213800) for financial support. R. M. Hernández-García wishes to thank CONACYT (Consejo Nacional de Ciencia y Tecnología) for a scholarship.

References

[1] F. Garcia-Romeu, Life Sci. 15 (1974) 539.
[2] K. Eskesen, H.H. Ussing, Acta Physiol. Scand. 136 (1989) 547.
[3] A. Pinelli, S. Trivulzo, L. Malvezzi, G. Rossoni, L. Beretta, Arzneim-Forsh 39 (1989) 467.
[4] G.R. Murthy, V.M. Reddy, Ind. J. Pharm. Sci. 49 (1987) 175.
[5] B. Serafin, G. Borlowska, J. Glowczyk, Y. Kowalska, S. Rump, Pol. J. Pharmacol. Pharm. 41 (1989) 89.
[6] N. Barba-Behrens, A. Ázquez-Olmos, S.E. Castillo-Blum, G. Höjer, S. Meza-Höjer, R.M. Hernández, M.deJ. Rosales-Hoz, R. Vicente, A. Escuer, Transition Met. Chem. 21 (1996) 31.
[7] N. Andrade-López, A. Ariza-Castolo, R. Contreras, A. Vázquez-Olmos, N. Barba-Behrens, H. Tlahuext, Heteroatom Chem. 8 (1997) 397.
[8] N. Andrade-López, R. Cartas-Rosado, E. García-Baéz, R. Contreras, H. Tlahuext, Heteroatom Chem. 9 (1998) 399.
[9] C. Acerete, J. Catalán, F. Fabero, M. Sánchez-Cabezudo, R.M. Claramunt, J. Elguero, Heterocycles 26 (1987) 1581.
[10] E. Grudemann, H. Graubaum, D. Martin, E. Schiewald, Magn. Reson. Chem. 24 (1986) 21.
[11] G.R. Bedford, P.J. Taylor, G.A. Webb, Magn. Reson. Chem. 33 (1995) 383.
[12] M.R. Caira, W.H. Watson, F. Vogtle, W. Müller, Acta Crystallogr. Sect. C40 (1984) 1047.
[13] W.H. Watson, J. Galloy, D.A. Grossie, J. Org. Chem. 49 (1984) 347.
[14] P.J. Steel, J. Heterocycl. Chem. 28 (1991) 1817.
[15] R. Zamorano-Ulloa, A. Vázquez-Olmos, N. Barba-Behrens, J. Inorg. Biochem. 51 (1993) 22.
[16] W.J. Hehre, L. Radom, P.V.R. Schleyer, J.A. Pople, Ab initio Molecular Orbital Theory, Wiley, New York, 1986.
[17] R.G. Parr, W. Yang, Density-Functional Theory of Atoms and molecules, Oxford University Press, New York, 1989.
[18] (a) J.P. Foster, F. Weinhold, J. Am. Chem. Soc. 102 (1980) 7211. (b) A.E. Reed, R.B. Weinstock, F. Weinhold, J. Chem.

Chem. Soc. 83 (1985) 735. (c) A.E. Reed, F. Weinhold, J. Chem. Phys. 83 (1985) 1736. (d) A.E. Reed, L.A. Curtiss, F. Weinhold, Chem. Rev. 88 (1989) 899.

[19] (a) A.A. Granovsky, PC GAMESS, V.6.2, 2001, http://classic.chem.msu.su/gran/gamess/index.html. (b) M.W. Schmit, K.K. Baldridge, J.A. Boatz, S.T. Elbert, M.S. Gordon, J.H. Jensen, S. Koseki, N. Matsunaga, K.A. Nguyen, S.J. Su, T.L. Windus, M. Dupuis, J.A. Montgomery, J. Comp. Chem., 14, 1993, pp. 1347.

[20] M.J. Frisch, G.W. Trucks, H.B. Schlegel, G.E. Scuseria, M.A. Robb, J.R. Cheeseman, V.G. Zakrzewski, J.A. Montgomery Jr., R.E. Stratmann, J.C. Burant, S. Dapprich, J.M. Millam, A.D. Daniels, K.N. Kudin, M.C. Strain, O. Farkas, J. Tomasi, V. Barone, M. Cossi, R. Cammi, B. Mennucci, C. Pomelli, C. Adamo, S. Clifford, J. Ochterski, G.A. Petersson, P.Y. Ayala, Q. Cui, K. Morokuma, D.K. Malick, A.D. Rabuck, K. Raghavachari, J.B. Foresman, J. Cioslowski, J.V. Ortiz, A.G. Baboul, B.B. Stefanov, G. Liu, A. Liashenko, P. Piskorz, I. Komaromi, R. Gomperts, R.L. Martin, D.J. Fox, T. Keith, M.A. Al-Laham, C.Y. Peng, A. Nanayakkara, C. Gonzalez, M. Challacombe, P.M.W. Gill, B. Johnson, W. Chen, M.W. Wong, J.L. Andres, C. Gonzalez, M. Head-Gordon, E.S. Replogle, J.A. Pople, GAUSSIAN 98, Revision A.7, Gaussian Inc., Pittsburg, PA, 1998.

[21] (a) C. Møller, M.S. Plesset, Phys. Rev. 46 (1934) 618. (b) J.S. Binkley, J.A. Pople, Int. J. Quantum Chem. (1975) 229.

[22] C. Lee, W. Yang, R.G. Parr, Phys Rev B 37 (1988) 785.

[23] E.D. Glendening, A.E. Reed, J.E. Carpenter, F. Weinhold, NBO 3.0 Theoretical Chemistry Institute, University of Wisconsin, Madison, 1990.

[24] (a) K.E. Gilbert, PCMODEL, Molecular Modeling Software, V.4.2, Serena Software, Bloomington, IN, 1990. (b) U. Burkert, N.L. Allinger, Molecular Mechanics, ACS Monograph 177, American Chemical Society, Washington, DC, 1982.

[25] (a) Leif Laaksonen, Center for Scientific Computing, Espoo, Finland, Version 2.0, 31-03-2001, http://www.csc.fi~laaksone/gopenmol (b) Graphic packages included in the distribution of GAMESS(US), http://www.msg.ameslab.gov/GAMESS/GAMESS.html page

[26] K.B. Wiberg, A. Murcko, J. Mol. Struct. 169 (1988) 355.

[27] (a) I. Mayer, Theor. Chim. Acta (Berl.) 67 (1985) 315. (b) I. Mayer, Int. J. Quantum Chem. 29 (1986) 73. (c) I. Mayer, Int. J. Quantum Chem. 29 (1986) 477.

[28] (a) R.S. Mulliken, J. Chem. Phys. 23 (1955) 1833. (b) R.S. Mulliken, J. Chem. Phys. 23 (1955) 1841. (c) R.S. Mulliken, J. Chem. Phys. 23 (1955) 2338. (d) R.S. Mulliken, J. Chem. Phys. 23 (1955) 2343.

[29] J.E. Del Bene, M.J. Frisch, K. Raghavachari, J.A. Pople, J. Phys. Chem. 86 (1982) 1529.

[30] (a) J. Catalan, J.L.G. de Paz, M. Yañez, J. Mol. Struct. (THEOCHEM) 107 (1984) 257. (b) J. Catalan, J.L.G. de Paz, M. Yañez, J. Elguero, J. Mol. Struct. (THEOCHEM) 108 (1984) 161.

[31] J.E. Del Bene, J. Am. Chem. Soc. 99 (1977) 3617.

[32] C. Ögretir, H. Berber, J. Mol. Struct. (THEOCHEM) 577 (2002) 197.

[33] P. Politzer, J.S. Murria, in: K.B. Lipkowsky, D.B. Boyd (Eds.), Reviews in Computational Chemistry, vol. 2, VCH, New York, 1991, (Chapter 7).